

GradPaint: Gradient-Guided Inpainting with Diffusion Models

Asya Grechka, Guillaume Couairon, Matthieu Cord
Sorbonne Université

{asya.grechka, guillaume.couairon, matthieu.cord}@isir.upmc.fr

Abstract

Denoising Diffusion Probabilistic Models (DDPMs) have recently achieved remarkable results in conditional and unconditional image generation. The pre-trained models can be adapted without further training to different downstream tasks, by guiding their iterative denoising process at inference time to satisfy additional constraints. For the specific task of image inpainting, the current guiding mechanism relies on copying-and-pasting the known regions from the input image at each denoising step. However, diffusion models are strongly conditioned by the initial random noise, and therefore struggle to harmonize predictions inside the inpainting mask with the real parts of the input image, often producing results with unnatural artifacts.

Our method, dubbed GradPaint, steers the generation towards a globally coherent image. At each step in the denoising process, we leverage the model’s “denoised image estimation” by calculating a custom loss measuring its coherence with the masked input image. Our guiding mechanism uses the gradient obtained from backpropagating this loss through the diffusion model itself. GradPaint generalizes well to diffusion models trained on various datasets, improving upon current state-of-the-art supervised and unsupervised methods. Our code will be made available upon publication.

1. Introduction

Inpainting consists in generating a missing part of a given image, given a binary mask indicating where the generation should take place. It is a fundamental task in computer vision, having obvious implications for image editing, image restoration, object removal, and so on. Currently, state-of-the-art methods are generally based on Generative Adversarial Networks (GANs) [37, 45], and consist in explicitly training a model to reconstruct an image using self-generated masks. Although these methods often achieve reasonable results with standard metrics, visual results tend to have obvious, unrealistic artifacts. Moreover, training these models is accompanied with the difficulties of train-

ing instability inherent with GANs as well as limitations on the diversity of the dataset distribution.

Denoising diffusion probabilistic models (DDPMs) have recently gained massive attention, achieving high-resolution, photo-realistic and diverse image generation [29, 11, 31, 1, 6, 27]. In terms of image generation, these models are on par or better than GANs even for constrained datasets like faces [31]; and largely surpass them for diverse datasets like ImageNet [27, 31]. Furthermore, recent models trained on large-scale datasets [11, 29, 27, 8, 31] have given rise to high-quality and flexible text-conditioned image generation, allowing users to generate astonishingly imaginative or artistic high-resolution images [35]. It is thus highly enticing to be able to use these pretrained models directly for downstream tasks, rather than re-training a new model from scratch. Here, we focus on the particular downstream task of inpainting.

There has been limited work in using pre-trained diffusion models for this task, and the typical approach [23, 26, 27] is to guide the generative model by replacing values of the intermediate noise map with noised pixels of the input image outside the inpainting mask, based on the hope that the denoising process inside the inpainting mask will progressively be biased towards image parts that blend naturally with the known surrounding context. However, this strategy often produces unsatisfying results, which we believe is due to the diffusion model being strongly conditioned on the initial noise map [17], therefore having difficulties harmonizing the generation when the initial random latent map is too mismatched with the input image.

In this paper, we propose a new strategy for guiding pre-trained diffusion models to better perform inpainting tasks. Our method, dubbed GradPaint, is optimizing the diffusion process by better harmonizing generated content inside the inpainting mask. This guides the generation at every single step of the denoising process towards a more harmonized final image. Our method aims to minimize or even eliminate all the artifacts and inconsistencies that generally persist on the images due to the masked regions. We propose a training-free algorithm which is advantageous because (i) there is no need to train a inpainting-

specialized model whenever a new model is available, and (ii) training-based methods must chose a mask distribution to train on, to which training-free methods are agnostic. We perform an extensive evaluation on various datasets, including CelebA-HQ[22], FFHQ[15], ImageNet[4], Places2[47], and COCO[20].

Our main contributions can be summed up as:

- We propose a novel training-free algorithm to the denoising scheduling of diffusion models for the specific task of inpainting. We improve this inpainting mechanism with the explicit goal of harmonizing the generated parts with the current context. Specifically, we use a custom *alignment loss* and leverage the intrinsic nature of diffusion models through which we back-propagate and calculate a gradient to optimize our loss.
- We show that our method generalizes well to a variety of datasets and pre-trained models, including latent-diffusion models. We show that our method improves baseline methods and is even on par with equivalent models trained specifically for the task of inpainting.

2. Related Work

2.1. Inpainting

Historically, inpainting was aimed at recovering small corruption errors in images and was addressed with matching or ‘‘borrowing’’ local color and texture around the masked region [28, 41]. Evaluation consisted in calculating a distance metric with respect to the unmasked image. More recently, generative models have become capable of synthesizing realistic and diverse images, allowing the use of much larger masks when inpainting images. Generative models thus have more freedom to ‘‘imagine’’ a wide range of possibilities much different from the reference image, which is satisfactory (and oftentimes desired) so long as the resulting output looks realistic.

In recent years, inpainting has been primarily addressed with training deep encoder-decoder convolutional networks from scratch, often using a GAN[9] loss to encourage plausibility. Most recent work consists in improving the typical convolutional architecture in the encoder and/or decoder to better leverage structural or textural information from the surrounding regions [37, 13, 43, 14, 42, 48, 21, 25, 46]. [18] proposes a progressive inpainting scheme which iteratively fills in the mask by using surrounding information in the deep feature space. [40, 19] propose a framework to locate and leverage semantic information.

In another line of work similar to ours, image completion is effectuated with the help of existing priors not specifically trained for the task. [39] trains a randomly initialized convolutional network to generate the input image, stopping

training before overfitting occurs. [30, 45, 2] utilize powerful pre-trained decoders like StyleGAN2[16] and only train encoders to map the input image into the latent space of the decoder, which can produce more realistic results if the input image fits well to the distribution of the pre-trained decoder.

2.2. Diffusion models

Diffusion models are becoming state-of the art methods for generation tasks on many modalities, like images, videos, speech and text. Their excellent scaling behavior makes them a model of choice for training on large and diverse data, compared to GANs which still suffer from mode collapse and training instabilities. They can also be conditioned on various input data: for the specific task of inpainting, the input image and mask can be given as additional input to train a conditional diffusion model specialized on the inpainting task, as done in [33].

However, due to the computational cost of training generative models, it is appealing to find adaptation algorithms for downstream tasks without fine-tuning, especially for the task of inpainting which bears a lot of similarities with the unconditional generation task. [31, 27, 36] propose to adapt pre-trained diffusion models to inpainting by injecting a guiding mechanism in the generative process, a strategy which we build upon in this paper. [23] also proposes to take advantage of pre-trained diffusion models with cycles of denoising and renoising operations, which we found computationally very expensive. Finally, in a parallel line of work most similar to ours, [3] similarly propose to guide the generation using the gradient of a ‘‘manifold constraint’’, but they do not use a custom loss nor do they apply optimization to the entirety of the intermediate noise maps.

3. GradPaint Method

3.1. Background

Denoising diffusion probabilistic models [12] is a class of generative models trained with the following image denoising objective:

$$\mathcal{L} = \mathbb{E}_{\mathbf{x}_0, t, \epsilon} \|\epsilon - \epsilon_\theta(\mathbf{x}_t, t)\|_2^2, \quad (1)$$

where ϵ_θ is a noise estimator network trained to predict the noise $\epsilon \sim \mathcal{N}(\mathbf{0}, \mathbf{I})$ mixed with an input image \mathbf{x}_0 in the following way: $\mathbf{x}_t = \sqrt{\alpha_t} \mathbf{x}_0 + \sqrt{1 - \alpha_t} \epsilon$. This training is performed for different values of the mixing coefficient α_t , monotonically decreasing from $\alpha_0 = 1$ (no noise) to $\alpha_T \simeq 0$ (almost pure noise) for a large integer T .

At inference time, a new sample from the training distribution can be obtained by starting from random Gaussian noise $\mathbf{x}_T \sim \mathcal{N}(\mathbf{0}, \mathbf{I})$, and iteratively refining it with the noise estimator network with the following equations, called *DDPM sampling equations* [12]:

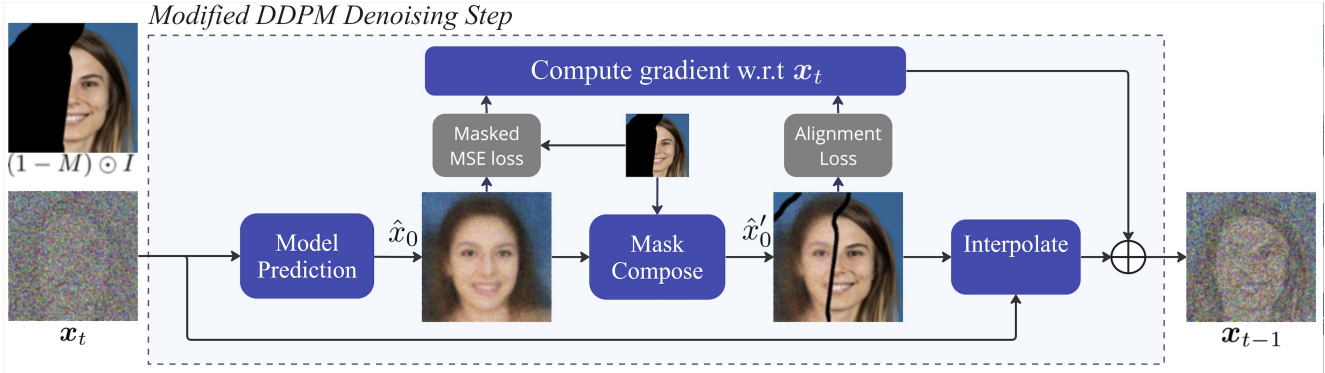


Figure 1. GradPaint method overview. We propose to modify one step of the DDPM denoising process with a gradient descent update on x_t to better match the masked input image, in turn producing a better matched noise map x_{t-1} for the next step. This improvement in the DDPM noise prediction thus allows for better fitting intermediate noise map predictions x_t earlier in the DDPM denoising process, which ultimately produces a successful final inpainted image x_0 .

x and \hat{x}

$$\begin{aligned} \hat{x}_0 &= \frac{1}{\sqrt{\alpha_t}} (x_t - \sqrt{1 - \alpha_t} \cdot \epsilon_\theta(x_t, t)), \\ x_{t-1} &= \frac{(\alpha_{t-1} - \alpha_t) \sqrt{\alpha_{t-1}}}{\alpha_{t-1}(1 - \alpha_t)} \hat{x}_0 + \frac{(1 - \alpha_{t-1}) \sqrt{\alpha_t}}{(1 - \alpha_t) \sqrt{\alpha_{t-1}}} x_t + \sigma z, \end{aligned} \quad (2)$$

where t goes from T to 0, σ_t is a variance parameter, and $z \sim \mathcal{N}(\mathbf{0}, \mathbf{I})$.

This iterative refinement can be “guided” to impose constraints on the generated sample x_0 . In the case of inpainting, the aim is that the generated image exactly matches the input image outside a given inpainting region. The variable \hat{x}_0 , available at each timestep, represents the model’s current estimation of what the denoised image will look at the end. For instance, [27] applies a maskwise correction on \hat{x}_0 at each timestep:

$$\hat{x}'_0 = M \odot \hat{x}_0 + (1 - M) \odot I, \quad (3)$$

where I is the input image and M is a binary image mask equal to 1 in the image regions that must be inpainted, 0 otherwise. The update rule for x_{t-1} is then adapted to use \hat{x}'_0 instead of \hat{x}_0 in Equation 2. This correction progressively biases the diffusion model to exactly match I outside the inpainting mask M . In the remaining of the paper, we refer to this method as *combine-image* since it combines the images \hat{x}_0 and I before interpolating with x_t .

Alternatively, [36, 31, 23] propose to directly correct x_{t-1} by replacing regions outside M with the noised regions of the input image I :

$$x'_{t-1} = M \odot x_{t-1} + (1 - M) \odot (\sqrt{\alpha_{t-1}} I + \sqrt{1 - \alpha_{t-1}} \epsilon), \quad (4)$$

where $\epsilon \sim \mathcal{N}(\mathbf{0}, \mathbf{I})$ is resampled at each step. This x'_{t-1} is then used as input for the next denoising step instead of x_{t-1} . We will refer to this method as *combine-noisy* since it combines x_{t-1} inside the mask with ground truth (noised) pixel values outside the mask.

3.2. GradPaint framework

Our strategy is built upon the *combine-image* zero-shot inpainting method presented in §3.1. Our key observation is that the most aesthetically-pleasing inpainting results are obtained when the collage $M \odot \hat{x}_0 + (1 - M) \odot I$ is coherent right from the beginning of the generation process. When this is not the case, there is a mismatch between the model’s estimation in the inpainting region and the known regions of input image I . This mismatch is generally present from the beginning and is not fully corrected during the denoising generation process.

To enforce harmonization between the inpainted region and known regions of the input image, we introduce the *GradPaint update*. An overview of our method is presented in Fig. 1. At each denoising step, the variable x_t is updated so that (i) \hat{x}_0 matches well known regions of I outside the mask; and (ii) the collage $M \odot \hat{x}_0 + (1 - M) \odot I$ does not present any discontinuity due to the copy-paste operation. This update consists in a one-step gradient descent update from two loss terms corresponding to the two objectives aforementioned.

Given a binary mask $M \in \mathbb{R}^{n \times n}$ and \odot denoting the element-wise product, we define our losses as follows:

Masked MSE loss. The first loss term is a mean squared error term outside the inpainting mask $(1 - M)$, taking as reference known regions of the input image:

$$\mathcal{L}_{mse}(I_1, I_2, M) = \frac{1}{n^2} \|I_1 \odot (1 - M) - I_2 \odot (1 - M)\|_2^2. \quad (5)$$

Alignment loss. The “alignment loss” $al(I, M)$ measures the smoothness of image I on the boundaries of the inpainting mask M . It is defined as follows:

$$al(I, M) = \frac{1}{n^2} \|D_x I \odot D_x (1 - M) + D_y I \odot D_y (1 - M)\|_2^2, \quad (6)$$

where D_x and D_y are the normalized image gradients:

$$\begin{bmatrix} D_x I \\ D_y I \end{bmatrix}_{(i,j)} = \begin{cases} \frac{\nabla I_{(i,j)}}{\|\nabla I_{(i,j)}\|_2}, & \text{if } \|\nabla I\|_{(i,j)} > 0 \\ [0 \ 0]^T, & \text{else} \end{cases} \quad (7)$$

with $\nabla I = [\partial_x I \ \partial_y I]^T$ is the vector of gradients of I in the x and y directions respectively. When we minimize this loss, we aim to achieve the smoothest transition possible in the image I along the direction where M changes values. Since this loss $al(I, M)$ is defined for an image with only one color channel, we simply define the total alignment loss \mathcal{L}_{al} as the average loss over the three color channels for a regular RGB image.

GradPaint Update. Our total loss is defined as:

$$\mathcal{L} = \mathcal{L}_{mse} + \lambda_{al} \mathcal{L}_{al}, \quad (8)$$

with λ_{al} being a hyperparameter controlling the relative strength of the alignment loss compared to the MSE loss.

At each step in the denoising process, we compute \mathbf{x}_{t-1} as a function of \mathbf{x}_t as in the *combine-image* method. In between each step, we update the variable \mathbf{x}_{t-1} with the normalized gradient of our total loss:

$$\mathbf{x}'_{t-1} = \mathbf{x}_{t-1} - \alpha \frac{\nabla_{\mathbf{x}_t} \mathcal{L}(\mathbf{x}_0, \hat{\mathbf{x}}_0, M)}{\|\nabla_{\mathbf{x}_t} \mathcal{L}(\mathbf{x}_0, \hat{\mathbf{x}}_0, M)\|_2}, \quad (9)$$

with α being a fixed learning rate.

Backpropagating through the diffusion model itself until variable \mathbf{x}_t is a crucial element of our method. Since \mathbf{x}_t is updated to produce a better estimation $\hat{\mathbf{x}}_0$ when processed by the diffusion model, this property will also transfer to \mathbf{x}_{t-1} which is, at each step, very close to \mathbf{x}_t .

3.3. Visualizations

Harmonization. The effect of the GradPaint update is illustrated in Fig. 2, which shows the intermediate DDPM predictions for $\hat{\mathbf{x}}_0$ and $\hat{\mathbf{x}}'_0$ at various timesteps. We compare GradPaint with the *combine-noisy* and *combine-image* methods presented in §3.1, where all three methods share the same DDPM model, parameters and initial noise maps. These baseline approaches require more steps to integrate the information from the input image, at which point it is often “too late” to construct a harmonized image - misalignment between the generation and the input image can no longer be corrected. In contrast, for GradPaint, the optimization step on \mathbf{x}_t quickly pushes the merged image $\hat{\mathbf{x}}'_0$ to harmonize well with the masked input image \mathbf{x}_0 , producing an inpainting result without alignment artifacts.

Gradient visualization. The two separate components of our loss have different effects on $\nabla \mathbf{x}_t$, as we can see in

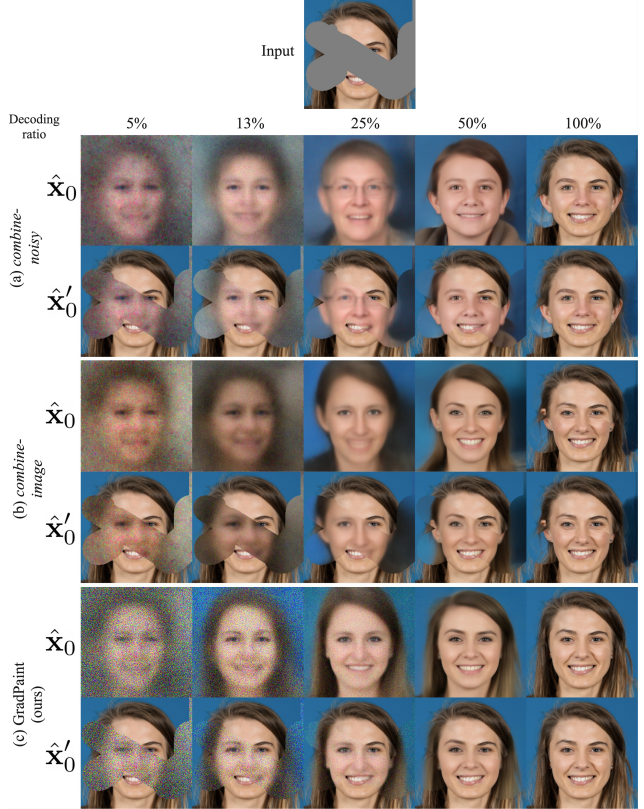


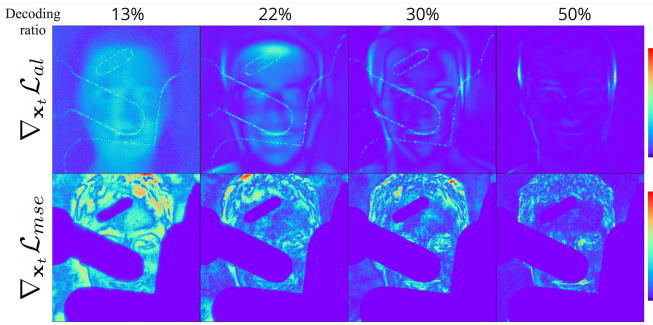
Figure 2. DDPM predictions at different stages (indicated in %) of the denoising process. We compare two baselines (a) and (b) with GradPaint (the two last rows). GradPaint better harmonizes regions inside and outside the inpainting mask right from the beginning of the denoising process.

Fig. 3a. While the gradient of the masked MSE loss remains active throughout the denoising process, the gradient of the alignment loss becomes obsolete about halfway-through, thereafter only concentrating in a few local points in \mathbf{x}_t . The gradient of the alignment loss has a concentrated effect on the borders of the mask, but also affects the entire noise map \mathbf{x}_t globally, while the masked MSE loss has a much stronger effect in the unmasked region. The alignment loss encourages smoother and more gradual transitions in the final generation, as can be seen with the background in Fig. 3b.

4. Evaluation Protocol

4.1. Pre-trained models and implementation details

We detail our setup for image-space diffusion models as well as latent-space diffusion models. We provide a detailed list of the assets used in our work (datasets, code, and models) in the Appendix in A.



(a) Gradient magnitude of different components of our losses with regards to x_t . The alignment loss has a concentrated effect at the border and a more global effect compared to the masked MSE loss, but dies out more quickly when it concentrates in a few local spots.

Figure 3. Effect of separate components of our loss on the intermediate predictions of the DDPM model and their corresponding gradients. Noise maps are initialized identically.

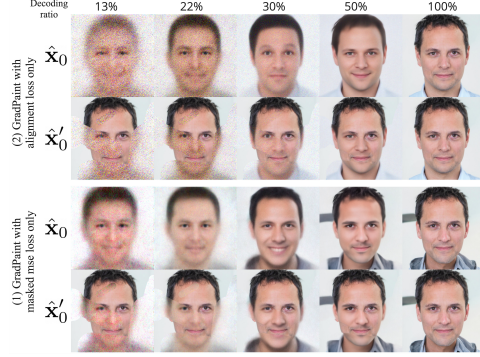
Experiments on image-space diffusion models We primarily use diffusion models from guided diffusion [7], which operates on images of size 256×256 . We use their pre-trained unconditional models (pre-trained on FFHQ, CelebAHQ, and Places2) as well as their class-conditional model trained on ImageNet.

We use a default number of 100 steps for DDPM sampling; the loss is computed with $\lambda_{al} = 400$ during the first 45 steps of decoding (and disabled afterwards following our observations shown in 3a). The gradient is updated with a fixed learning rate of 0.005.

Extension to latent diffusion models We also experiment with latent diffusion models [32]. We have observed that the latent spaces that we use have much less structure compared to real images, and that our alignment loss, whose role is to enforce smoothness on real images, cannot fulfill this role in latent spaces. Therefore, for all experiments with latent diffusion models, we only experiment with the masked MSE loss, which naturally extends to latent spaces by considering the encoded input image as reference in our MSE loss.

Latent diffusion models also operate on 256×256 images, but images are edited in a latent space with spatial dimensions of 64×64 . We use pre-trained unconditional latent diffusion models on CelebAHQ and FFHQ. We use the class-conditional latent diffusion model pre-trained on ImageNet. Finally, for text-conditional models, we use Stable Diffusion pre-trained on the public LAION-5B dataset [34].

We use a default number of 100 steps for DDPM sampling; the loss is computed with $\lambda_{mse} = 1$. The gradient is updated with a fixed learning rate of 0.005.



(b) Intermediate DDPM predictions with GradPaint using separate components of our loss. The alignment loss encourages smooth and coherent transitions, as can be seen with the homologous background.

Datasets We evaluate our algorithm on five datasets: FFHQ, CelebAHQ, ImageNet, Places2 and COCO.

Given an image, the aim is to perform inpainting inside a random mask generated with the mask generator from [37]. We mainly evaluate on the difficult and more realistic *thick* masks (additional results on *thin* and *medium* masks are provided in the appendix). We create 5000 masked images for all experiments.

For both image-space and latent diffusion models, we evaluate the FFHQ pre-trained model on a subset of CelebAHQ images. Inversely, we evaluate the CelebAHQ pre-trained model on a subset of FFHQ images. We evaluate the ImageNet pre-trained models on a subset ImageNet validation set and use the class label as conditioning.

For the image-space diffusion model pre-trained on Places2, we use a subset of the Places2 validation set for evaluation. For the Stable Diffusion model pre-trained on LAION-5B, we use a subset of the COCO validation set and use the captions as conditioning text information for the diffusion model.

4.2. Metrics

For a set of images inpainted with a given method, we compute two core metrics that encapsulate the challenges of inpainting: the LPIPS distance [44] between the inpainted image and the (unmasked) input image which measures the extent to which we correctly recover the masked regions, and the FID score [10] which measures the realism of output images. The primary requirement is that inpainted images should look as natural as possible, hence having the smallest possible FID score. For LPIPS distances, an inpainting result closer to the reference image is generally better, although realistic images further away from the reference image can also be satisfactory, especially for large masks.

Dataset	FFHQ		CelebaHQ	
Metrics	FID \downarrow	LPIPS \downarrow	FID \downarrow	LPIPS \downarrow
COPY (oracle)	4.29	0	3.01	0
GREYFILL	78.08	0.257	96.41	0.264
LaMa	6.27	0.076	n/a	n/a
Palette	7.28	0.096	n/a	n/a
Repaint	9.09	0.090	8.44	0.078
MCG	<u>6.17</u>	0.097	6.67	0.084
<i>combine-noisy</i>	9.04	0.119	9.89	0.103
<i>combine-image</i>	7.30	0.123	<u>5.83</u>	0.110
GradPaint (ours)	5.65	<u>0.084</u>	4.41	0.077

Table 1. Evaluation of various methods on FFHQ and CelebaHQ datasets. The COPY oracle and the GREYFILL measure are respectfully the lower and upper bounds for LPIPS and FID. LaMa and Palette are both training-based methods. Repaint, *combine-noisy*, *combine-image*, MCG and GradPaint are all training-free methods which all use the same model based on guided diffusion[6]. Best score is shown in **bold** and second best underlined. As we can see, our method produces the best results in terms of FID and is on-par with fully-supervised methods in terms of LPIPS.

4.3. Baselines

We compute the best and worst possible LPIPS and FID scores with two trivial measures: the *COPY* oracle measure, which simply copies the (unmasked) input image, gives an LPIPS score of 0 and a lower bound on possible FID scores; and the *GREYFILL* measure, which simply fills the region to be inpainted with uniform grey. We also add a *Latent COPY* oracle for latent diffusion models which consists in simply auto-encoding the input image. Without gradient-based optimization, our method is equivalent to the *combine-image* baseline for image inpainting, which we evaluate in our experiments along with its *combine-noisy* variant. Apart from these three closely related methods, we compare against the following state-of-the-art inpainting methods: LaMa [37], a GAN-based method trained for inpainting; Palette [33], also trained for inpainting but with diffusion models, RePaint [24], another training-free inpainting algorithm that is much more computationally expensive, and finally MCG [3], a parallel line of work to ours which is similarly training-free but with a different optimization scheme.

5. Quantitative Evaluation

Image-space Diffusion Models Quantitative results on the FFHQ and CelebA datasets for image-space diffusion models are shown in Tab. 1, where GradPaint is compared against available competing methods (FFHQ-pretrained checkpoints are not available for Palette and LAMA) as well as the *combine* baselines. We present the

Method	FID \downarrow	LPIPS \downarrow
<i>combine-noisy</i>	10.33	0.1907
<i>combine-image</i>	9.61	0.1797
GradPaint w/o alignment loss	8.12	0.1551
GradPaint	7.86	0.1486

Table 2. Detailed comparison on ImageNet pre-trained guided diffusion model with *thick* masks.

results for the *thick* mask setting, as this is the most interesting setting for practical applications. Results for other mask sizes are presented in the appendix. The benefit of our gradient update is visible when comparing to *combine-image* (same as ours without gradient updates): On FFHQ, the FID score is reduced from 7.30 to 5.65, a significant improvement given that the minimum obtainable FID score is 4.29 on 5000 images (*COPY* oracle measure). Results on both datasets show similar gains. When comparing with competing methods on FFHQ, GradPaint obtains the state-of-the art FID score, outperforming methods specialized in inpainting (Palette, LAMA) as well as the training-free algorithms Repaint and MCG based on the same diffusion model as ours. LaMa obtains slightly better LPIPS scores but requires an inpainting-specific training (compared to simply using a pre-trained generative model). Moreover, LaMa, unlike all other methods, has access at train time to the mask distribution that we use for testing.

We validate different components of our method with the ImageNet [5] dataset and guided diffusion model, summarized in Tab. 2. This more difficult dataset was chosen to better analyze our different components as well as validate our method on class-conditioned diffusion models, where generation could be biased by the class. Our full method, and the alignment loss in particular, improves reconstruction and realism of generated images.

Latent Diffusion Models Results on Latent Diffusion Models are presented in Tab. 3. As we can see, the latent space allows for very good image reconstruction (small LPIPS scores), so it is not a real limitation and GradPaint (latent) is still able to outperform competing methods (FID 5.97 on FFHQ *thick* masks). Overall, we observe large and consistent gains on all three datasets ImageNet, COCO and FFHQ datasets over the reference inpainting methods, for both FID and LPIPS.

6. Qualitative Evaluation

Image-space Diffusion Models Figs. 4 and 5 and show qualitative results using our method for Places2 and ImageNet pre-trained models, respectfully. Note that without the gradient-guidance of GradPaint, generations are unable to harmonize well. Images produced by RePaint [24] often lack global coherence, like the missing spider web in Fig. 4.

Dataset	ImageNet		COCO		FFHQ	
	FID	LPIPS	FID	LPIPS	FID	LPIPS
COPY (o.)	12.27	0.0	7.29	0.0	4.29	0.0
Lat. COPY (o.)	12.00	0.034	7.71	0.041	4.98	0.018
GREYFILL	34.51	0.269	29.97	0.264	77.43	0.257
combine-noisy	17.17	0.195	11.12	0.241	8.73	0.132
combine-image	17.37	0.207	12.68	0.257	6.832	0.127
GradPaint (ours)	14.62	0.163	9.43	0.216	5.97	0.111

Table 3. Evaluation of pre-trained latent diffusion models with *thick* masks. For all values, lower is better. The COPY oracle measures the metrics on the ground-truth images, and the Latent COPY oracle does the same for autoencoded ground-truth images. As we can see, our modification for latent diffusion models yields significant improvements on all datasets.

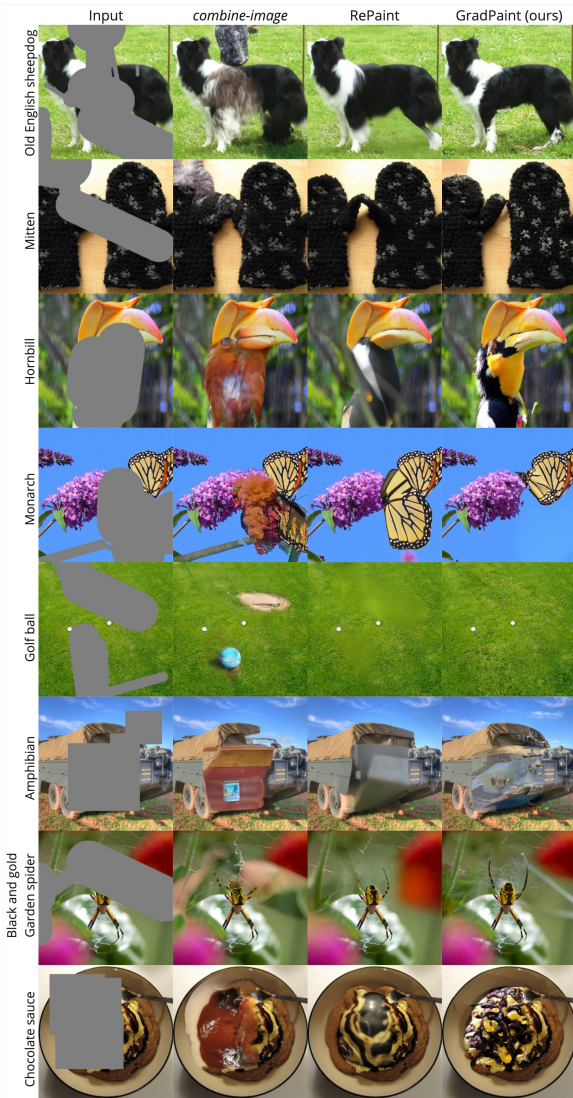


Figure 4. Inpainting results on select images from ImageNet. The *combine-image* baseline produces unharmonized results and struggles to take the context into account. Our method produces high-quality results at a fraction of the time of RePaint[23].

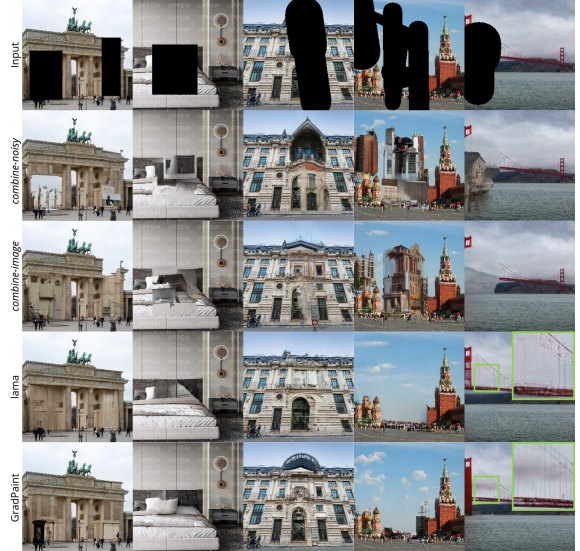


Figure 5. In-the-wild images for models trained on Places2. Note that *combine-image*, *combine-noisy* and GradPaint all use the same noise map for initialization. Note that LaMa was specifically trained using similar masks, contrary to our method.

Our method produces globally and locally harmonized images, without the heavy computation cost of [24] nor the specific supervised training of [37]. Note that we selected images where the *thick* masks masked out key parts of the input image to better appreciate the different results.

Fig. 6 shows qualitative results on ImageNet-trained guided diffusion model for different components of our method. We note that the baseline *combine-image* is biased by the class-conditioning of the model without taking into account the context, like for the “red wolf” class. Adding gradient update as well as the alignment loss produces generations harmonized with the surrounding context.

Latent Diffusion Models Fig. 7 shows visual examples of our method using Stable Diffusion on COCO. Our method produces realistic and harmonized results compared to the baseline method. We provide further results on ImageNet in the Appendix E.

7. Impact of mask distribution

Training-free is particularly advantageous as such a method is agnostic to any pre-defined mask distribution to train on, contrary to training-based methods. We illustrate this by comparing our method to [37] on masks outside of their pre-defined training distribution. Specifically, we create masks where each pixel has a 80% chance of being masked, masking considerable portions of the image. As we can see in Fig. 8, [37] produces low-quality results while our method produces realistic images. This is confirmed quantitatively in Tab. 4.

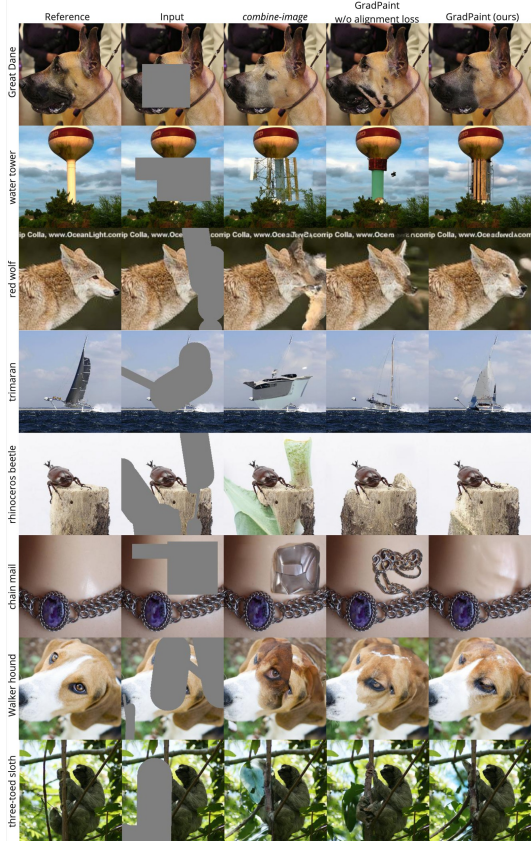


Figure 6. Qualitative results for select images of ImageNet dataset. Baseline *combine-image* produces images with visible artifacts. Our gradient update using only the masked MSE loss improves the “copy-paste” effect, while the alignment loss produces better aligned transitions.

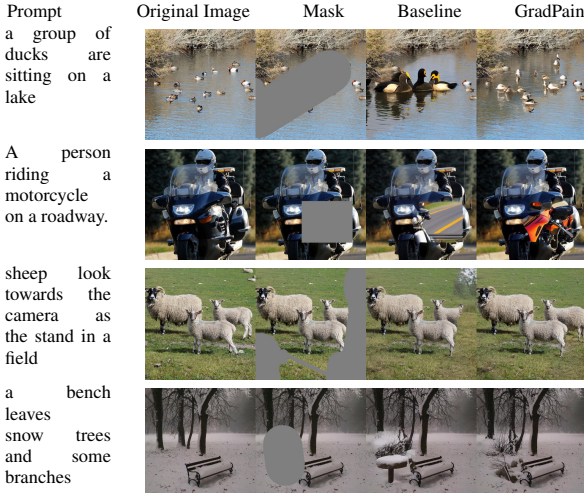


Figure 7. Qualitative results using Stable Diffusion on COCO. As we can see, our method successfully corrects unharmonized inpainted images.



Figure 8. Uncurated results of our method compared to LaMa on out-of-distribution masks. We show images from (a) FFHQ and (b) Places2. LaMa fares poorly on masks outside of the training distribution. Best viewed zoomed and in color.

	CelebaHQ		Places2	
	FID \downarrow	LPIPS \downarrow	FID \downarrow	LPIPS \downarrow
COPY (oracle)	4.29	0.0	6.47	0.0
GREYFILL	403.23	1.06	282.01	1.09
LaMa	74.47	0.517	52.63	0.320
GradPaint	44.87	0.170	27.17	0.277

Table 4. Quantitative results comparing our train-free method to a training-based method (LaMa) on CelebaHQ and Places2 using masks outside of LaMa’s training distribution.

8. Conclusion

We have presented GradPaint, a training-free algorithm that guides the generative process of diffusion to better perform inpainting operations when given real images. GradPaint improves upon baselines by better harmonizing generated content inside the inpainting mask with known regions of the input image, which is done via gradient descent computed from a dedicated harmonization loss. Extensive qualitative and quantitative experiments demonstrate the superiority of our method, which is able to outperform methods trained specifically for inpainting.

It is important to note that many open-source diffusion models are trained with large amounts of web-scraped data, thus inheriting their biases. Applying our method onto these models could potentially reinforce harmful cultural biases. We believe open-sourcing editing algorithms in a research context contributes to a better understanding of these biases and will aid the community to mitigate them in the future.

References

[1] Andreas Blattmann, Robin Rombach, Kaan Oktay, and Björn Ommer. Retrieval-augmented diffusion models. *arXiv preprint arXiv:2204.11824*, 2022. 1

[2] Kelvin CK Chan, Xintao Wang, Xiangyu Xu, Jinwei Gu, and Chen Change Loy. Glean: Generative latent bank for large-factor image super-resolution. In *CVPR*, 2021. 2

[3] Hyungjin Chung, Byeongsu Sim, and Jong Chul Ye. Improving diffusion models for inverse problems using manifold constraints. In *NeurIPS*, 2022. 2, 6

[4] Jia Deng, Wei Dong, Richard Socher, Li-Jia Li, Kai Li, and Li Fei-Fei. Imagenet: A large-scale hierarchical image database. In *CVPR*, 2009. 2

[5] J. Deng, W. Dong, R. Socher, L.-J. Li, K. Li, and L. Fei-Fei. Imagenet: A large-scale hierarchical image database. In *CVPR*, 2009. 6

[6] Prafulla Dhariwal and Alexander Nichol. Diffusion models beat gans on image synthesis. In *NeurIPS*, 2021. 1, 6

[7] Prafulla Dhariwal and Alexander Quinn Nichol. Diffusion models beat GANs on image synthesis. In *NeurIPS*, 2021. 5

[8] Oran Gafni, Adam Polyak, Oron Ashual, Shelly Sheynin, Devi Parikh, and Yaniv Taigman. Make-a-scene: Scene-based text-to-image generation with human priors. In *ECCV*, 2022. 1

[9] Ian Goodfellow, Jean Pouget-Abadie, Mehdi Mirza, Bing Xu, David Warde-Farley, Sherjil Ozair, Aaron Courville, and Yoshua Bengio. Generative adversarial nets. In *NeurIPS*, 2014. 2

[10] Martin Heusel, Hubert Ramsauer, Thomas Unterthiner, Bernhard Nessler, and Sepp Hochreiter. Gans trained by a two time-scale update rule converge to a local nash equilibrium. *NeurIPS*, 2017. 5

[11] Jonathan Ho, William Chan, Chitwan Saharia, Jay Whang, Ruiqi Gao, Alexey Gritsenko, Diederik P. Kingma, Ben Poole, Mohammad Norouzi, David J. Fleet, and Tim Salimans. Imagen video: High definition video generation with diffusion models. *arXiv preprint arXiv:2210.02303*, 2022. 1

[12] Jonathan Ho, Ajay Jain, and Pieter Abbeel. Denoising diffusion probabilistic models. *NeurIPS*, 33:6840–6851, 2020. 2

[13] Xin Hong, Pengfei Xiong, Renhe Ji, and Haoqiang Fan. Deep fusion network for image completion. In *Proceedings of the 27th ACM international conference on multimedia*, pages 2033–2042, 2019. 2

[14] Håkon Hukkelås, Frank Lindseth, and Rudolf Mester. Image inpainting with learnable feature imputation. In *DAGM German Conference on Pattern Recognition*, pages 388–403. Springer, 2020. 2

[15] Tero Karras, Samuli Laine, and Timo Aila. Flickr faces hq (ffhq) 70k from stylegan. *CoRR*, 2018. 2

[16] Tero Karras, Samuli Laine, Miika Aittala, Janne Hellsten, Jaakko Lehtinen, and Timo Aila. Analyzing and improving the image quality of stylegan. In *CVPR*, 2020. 2

[17] Valentin Khrulkov, Gleb Ryzhakov, Andrei Chertkov, and Ivan Oseledets. Understanding DDPM latent codes through optimal transport. In *ICLR*, 2023. 1

[18] Jingyuan Li, Ning Wang, Lefei Zhang, Bo Du, and Dacheng Tao. Recurrent feature reasoning for image inpainting. In *CVPR*, 2020. 2

[19] Liang Liao, Jing Xiao, Zheng Wang, Chia-Wen Lin, and Shin’ichi Satoh. Guidance and evaluation: Semantic-aware image inpainting for mixed scenes. In *ECCV*, 2020. 2

[20] Tsung-Yi Lin, Michael Maire, Serge J. Belongie, Lubomir D. Bourdev, Ross B. Girshick, James Hays, Pietro Perona, Deva Ramanan, Piotr Dollár, and C. Lawrence Zitnick. Microsoft COCO: common objects in context. *CoRR*, abs/1405.0312, 2014. 2

[21] Guilin Liu, Fitzsum A Reda, Kevin J Shih, Ting-Chun Wang, Andrew Tao, and Bryan Catanzaro. Image inpainting for irregular holes using partial convolutions. In *ECCV*, 2018. 2

[22] Ziwei Liu, Ping Luo, Xiaogang Wang, and Xiaoou Tang. Deep learning face attributes in the wild. In *ICCV*, 2015. 2

[23] Andreas Lugmayr, Martin Danelljan, Andrés Romero, Fisher Yu, Radu Timofte, and Luc Van Gool. Repaint: Inpainting using denoising diffusion probabilistic models. *CVPR*, 2022. 1, 2, 3, 7

[24] Andreas Lugmayr, Martin Danelljan, Andres Romero, Fisher Yu, Radu Timofte, and Luc Van Gool. Repaint: Inpainting using denoising diffusion probabilistic models. In *Proceedings of the IEEE/CVF Conference on Computer Vision and Pattern Recognition*, pages 11461–11471, 2022. 6, 7, 12

[25] Yuqing Ma, Xianglong Liu, Shihao Bai, Lei Wang, Aishan Liu, Dacheng Tao, and Edwin R Hancock. Regionwise generative adversarial image inpainting for large missing areas. *IEEE Transactions on Cybernetics*, 2022. 2

[26] Chenlin Meng, Yutong He, Yang Song, Jiaming Song, Jiajun Wu, Jun-Yan Zhu, and Stefano Ermon. SDEdit: Guided image synthesis and editing with stochastic differential equations. In *ICLR*, 2022. 1

[27] Alex Nichol, Prafulla Dhariwal, Aditya Ramesh, Pranav Shyam, Pamela Mishkin, Bob McGrew, Ilya Sutskever, and Mark Chen. GLIDE: towards photorealistic image generation and editing with text-guided diffusion models. In *ICML*, 2022. 1, 2, 3

[28] Patrick Perez, Michel Gangnet, and Andrew Blake. Poisson image editing. *ACM Trans. Graph.*, 2003. 2

[29] Aditya Ramesh, Prafulla Dhariwal, Alex Nichol, Casey Chu, and Mark Chen. Hierarchical text-conditional image generation with clip latents. *arXiv preprint arXiv:2204.06125*, 2022. 1

[30] Elad Richardson, Yuval Alaluf, Or Patashnik, Yotam Nitzan, Yaniv Azar, Stav Shapiro, and Daniel Cohen-Or. Encoding in style: a stylegan encoder for image-to-image translation. In *CVPR*, 2021. 2

[31] Robin Rombach, Andreas Blattmann, Dominik Lorenz, Patrick Esser, and Björn Ommer. High-resolution image synthesis with latent diffusion models. In *CVPR*, 2022. 1, 2, 3

[32] Robin Rombach, Andreas Blattmann, Dominik Lorenz, Patrick Esser, and Björn Ommer. High-resolution image synthesis with latent diffusion models. In *Proceedings of the IEEE/CVF Conference on Computer Vision and Pattern Recognition*, pages 10684–10695, 2022. 5

[33] Chitwan Saharia, William Chan, Huiwen Chang, Chris Lee, Jonathan Ho, Tim Salimans, David Fleet, and Mohammad Norouzi. Palette: Image-to-image diffusion models. In *ACM SIGGRAPH*, 2022. 2, 6

[34] Christoph Schuhmann, Romain Beaumont, Richard Vencu, Cade Gordon, Ross Wightman, Mehdi Cherti, Theo Coombes, Aarush Katta, Clayton Mullis, Mitchell Wortsman, et al. Laion-5b: An open large-scale dataset for training next generation image-text models. In *NeurIPS*, 2022. 5

[35] Sincarnate. The picture drawn by the image generation ai “midjourney” took first place at the art competition and the human artist was furious – gigazine. <https://japan.postsen.com/art/24187/The-picture-drawn-by-the-image-generation-AI-Midjourney-took-first-place-at-the-art-competition-and-E2%80%93-GIGAZINE.html>. Accessed: 2022-11-08. 1

[36] Yang Song, Jascha Sohl-Dickstein, Diederik P Kingma, Abhishek Kumar, Stefano Ermon, and Ben Poole. Score-based generative modeling through stochastic differential equations. In *ICLR*, 2021. 2, 3

[37] Roman Suvorov, Elizaveta Logacheva, Anton Mashikhin, Anastasia Remizova, Arsenii Ashukha, Aleksei Silvestrov, Naejin Kong, Harshith Goka, Kiwoong Park, and Victor Lempitsky. Resolution-robust large mask inpainting with fourier convolutions. In *Proceedings of the IEEE/CVF Winter Conference on Applications of Computer Vision*, pages 2149–2159, 2022. 1, 2, 5, 6, 7

[38] Christian Szegedy, Vincent Vanhoucke, Sergey Ioffe, Jon Shlens, and Zbigniew Wojna. Rethinking the inception architecture for computer vision. In *CVPR*, 2016. 12

[39] Dmitry Ulyanov, Andrea Vedaldi, and Victor Lempitsky. Deep image prior. In *CVPR*, 2018. 2

[40] Wei Xiong, Jiahui Yu, Zhe Lin, Jimei Yang, Xin Lu, Connelly Barnes, and Jiebo Luo. Foreground-aware image inpainting. In *CVPR*, 2019. 2

[41] Zongben Xu and Jian Sun. Image inpainting by patch propagation using patch sparsity. *IEEE Transactions on Image Processing*, 2010. 2

[42] Jie Yang, Zhiqian Qi, and Yong Shi. Learning to incorporate structure knowledge for image inpainting. In *AAAI*, 2020. 2

[43] Tao Yu, Zongyu Guo, Xin Jin, Shilin Wu, Zhibo Chen, Weiping Li, Zhizheng Zhang, and Sen Liu. Region normalization for image inpainting. In *AAAI*, 2020. 2

[44] Richard Zhang, Phillip Isola, Alexei A Efros, Eli Shechtman, and Oliver Wang. The unreasonable effectiveness of deep features as a perceptual metric. In *CVPR*, 2018. 5

[45] Shengyu Zhao, Jonathan Cui, Yilun Sheng, Yue Dong, Xiao Liang, Eric I Chang, and Yan Xu. Large scale image completion via co-modulated generative adversarial networks. In *ICLR*, 2021. 1, 2

[46] Haitian Zheng, Zhe Lin, Jingwan Lu, Scott Cohen, Eli Shechtman, Connelly Barnes, Jianming Zhang, Ning Xu, Sohrab Amirghodsi, and Jiebo Luo. Cm-gan: Image inpainting with cascaded modulation gan and object-aware training. *arXiv preprint arXiv:2203.11947*, 2022. 2

[47] Bolei Zhou, Agata Lapedriza, Aditya Khosla, Aude Oliva, and Antonio Torralba. Places: A 10 million image database for scene recognition. *IEEE Transactions on Pattern Analysis and Machine Intelligence*, 2017. 2

[48] Manyu Zhu, Dongliang He, Xin Li, Chao Li, Fu Li, Xiao Liu, Errui Ding, and Zhaoxiang Zhang. Image inpainting by end-to-end cascaded refinement with mask awareness. *IEEE Transactions on Image Processing*, 30:4855–4866, 2021. 2

A. Details on Assets

Table 5 (links) and Table 6 (licences) list the assets we used in this work.

Asset Name	Link
CelebA	https://mmlab.ie.cuhk.edu.hk/projects/CelebA.html
FFHQ	https://github.com/NVlabs/ffhq-dataset
Places2	http://places2.csail.mit.edu/download.html
ImageNet	https://www.image-net.org
COCO	https://cocodataset.org/
Guided Diffusion	https://github.com/openai/guided-diffusion
Latent Diffusion	https://github.com/CompVis/latent-diffusion
Stable Diffusion	https://github.com/CompVis/stable-diffusion
LaMa	https://github.com/advimman/lama
Palette	https://github.com/Janspiry/Palette-Image-to-Image-Diffusion-Models
LPIPS	https://github.com/richzhang/PerceptualSimilarity
FID	https://github.com/mseitzer/pytorch-fid
FFHQ pre-trained model	https://github.com/yandex-research/ddpm-segmentation
RePaint	https://github.com/andreas128/RePaint
MCG	https://github.com/HJ-harry/MCG_diffusion

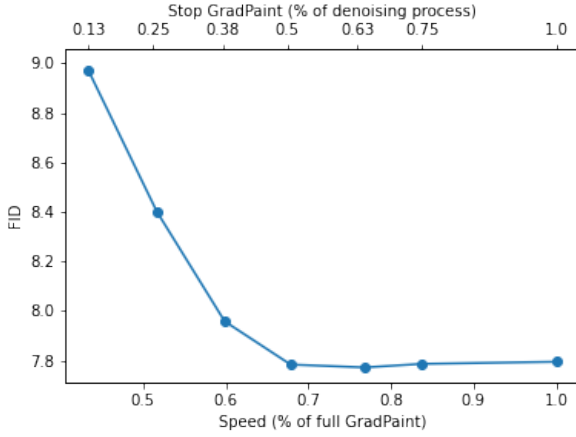
Table 5. List of asset links.

Asset Name	Asset type	License
CelebA	Images	CC BY-NC-SA 4.0 License
FFHQ	Images	https://github.com/NVlabs/ffhq-dataset/blob/master/LICENSE.txt
Places2	Images	Creative Commons Attribution 4.0 International
ImageNet	Images	https://www.image-net.org/download.php
COCO	Images	Creative Commons Attribution 4.0 License
Guided Diffusion	Code and Models	MIT License
Latent Diffusion	Code and Models	MIT License
Stable Diffusion	Code and Model	CreativeML Open RAIL-M
LaMa	Code and Models	Apache License 2.0
Palette	Code and Models	MIT License
LPIPS	Code and Models	BSD-2-Clause License
FID	Code and Models	Apache-2.0 License
FFHQ pre-trained model	Model	MIT License
RePaint	Code	CC BY-NC-SA 4.0 License
MCG	Code	Apache License 2.0

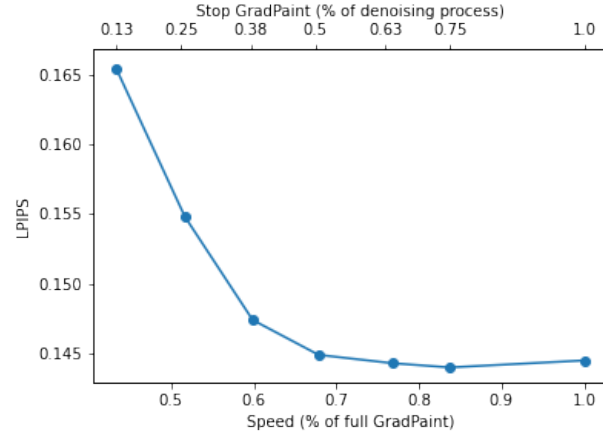
Table 6. List of asset licenses.

B. Inference Time Study

Our method requires approximately 3x the compute time of the gradient-free sampling baselines *combine-image* and *combine-noisy*, explained by the added backpropagation of every step of the denoising process. As illustrated in Fig. 2, our method succeeds because the prediction \hat{x}_0 is aligned and harmonized with the input image early on in the denoising process. We can improve the time of GradPaint by early-stopping the gradient calculation and letting the rest of the denoising process run as in *combine-image*. If the harmonization succeeded well-enough early on, then subsequent gradient calculations may not be necessary later in the denoising process, saving valuable compute time. We performed these experiments for various early stopping times of the total denoising process. Fig. 9 shows the performance in terms of LPIPS and FID for the various settings. Performing GradPaint after 63% of the denoising process doesn't improve performance, and significantly increases compute time. Stopping the gradient calculation at about 50% of the denoising process achieves the most important gains in performance and allows us to reduce the initial GradPaint time by 33%. This early stopping is referred to as "GradPaint-Fast" below.



(a) FID vs. Time tradeoff



(b) LPIPS vs. Time tradeoff

Figure 9. Performance vs. Time tradeoff, performed on ImageNet. We performed various settings where we early stopped the gradient calculation of GradPaint at 13%, 25%, 38%, 50%, 63%, 75% of the denoising process. The most important gains of GradPaint occurs thanks to the early gradient-guidance, and after 63%, gradient guiding no longer helps performance. A reasonable early-stopping at 50% of the denoising process reduces the initial time of GradPaint by 33%.

Lastly, we compare the inference times of various methods in Table 7. Our method is faster than other diffusion-based methods, even those specifically trained for inpainting (Palette), especially when applied to LDMs. We remark that RePaint [24] takes 313s (over 5 minutes!) per image, making it unfitting for practical use.

Method	Training-Free?	Diffusion-based?	Inference time per image (s)
LaMa			0.02
Palette		✓	56
RePaint	✓	✓	313
MCG	✓	✓	52
GradPaint	✓	✓	66
GradPaint-Fast	✓	✓	44
GradPaint-Latent	✓	✓	7.2

Table 7. Inference times for various methods. As we can see, our method is faster than other diffusion-based methods, especially when applied to Latent Diffusion Models

C. Inpainting with diversity

A method which well-harmonizes an image for the inpainting task will, naturally, produce less diverse images. This can be illustrated in Fig. 10. Because the baseline method poorly utilizes the surrounding context, samples are diverse but not realistic. On the other hand, our method leverages the surrounding context which produces a more natural result, implying more consistent generations. To further analyze the diversity of our samples, we used one single input image and generated 500 outputs, comparing our method with the baseline *combine-image*. We then extracted image features using the inception v3 pre-trained model [38] and display the average of the variance of these features. Tab. 8 shows the results. Our method gives diverse samples as the input mask sizes increases, but limits absurd and unharmonized results.

D. Additional Quantitative and Qualitative Results

Tab. 9 compares various training-based (LaMa and Palette) and training-free (Repaint, *combine-noisy*, *combine-image* MCG and GradPaint (ours)) methods for *thin* and *medium* masks which LaMa used for training. As we can see, our method generally achieves the best FID score and a comparable LPIPS score even with LaMa’s fully supervised method.

Figs. 11 and 12 show additional qualitative examples using *thin* and *medium* masks. With these smaller masks, the visual differences are sometimes harder to appreciate, and we recommend zooming when viewing results. We compare our method

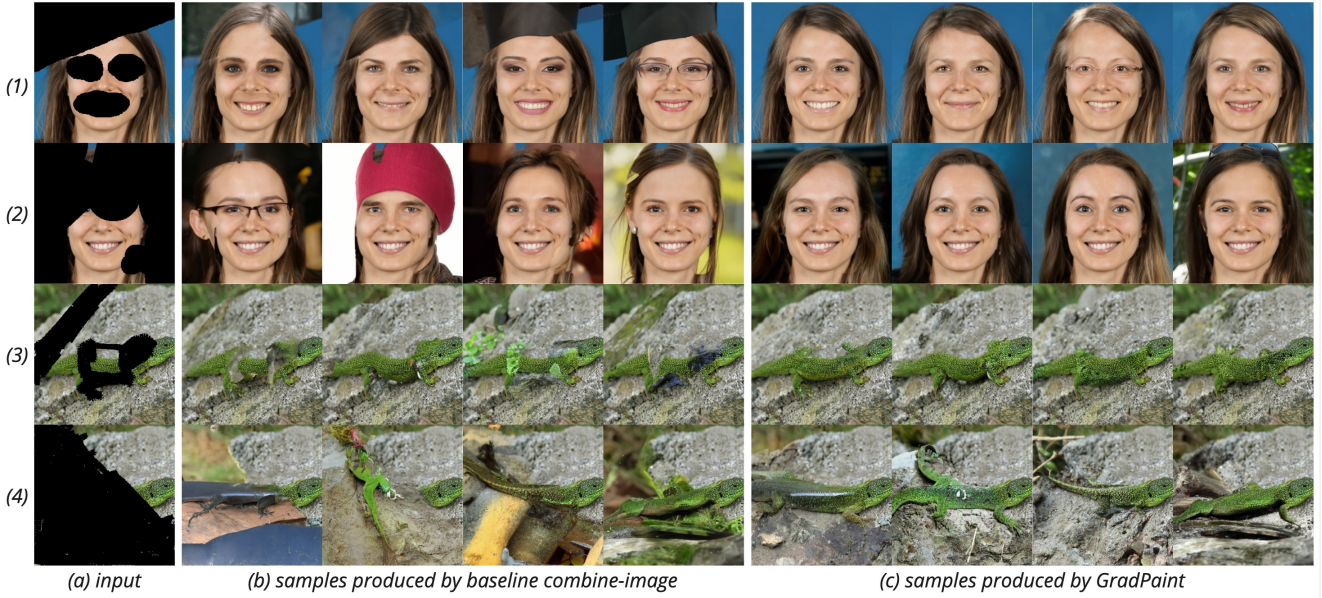


Figure 10. Diversity of select samples from 30 random samples. Images which are well-harmonized are less diverse, e.g. in (1), our method is encouraged to produce a blue background using the small available context, disregarded by the baseline method which produces more diverse but unharmonized backgrounds. Matching columns of samples of (b) and (c) are initialized identically.

mask coverage (% of im.)	10%	25%	50%	75%
combine-image	2.3	5.5	10.5	11.9
GradPaint	1.9	4.4	8.7	9.6

Table 8. Variance of image features (in 10^{-3}) for GradPaint compared to the baseline method, for 500 generated results using the same input image and increasing-sized masks. Our method expectedly produces more diverse images as the inpainting mask increases, nearing the diversity of the baseline for large masks.

Dataset	FFHQ (pretrained on CelebaHQ)				CelebaHQ (pretrained on FFHQ)					
	Masks		Thin		Medium		Thin		Medium	
Metrics	FID \downarrow	LPIPS \downarrow	FID \downarrow	LPIPS \downarrow	FID \downarrow	LPIPS \downarrow	FID \downarrow	LPIPS \downarrow	FID \downarrow	LPIPS \downarrow
COPY (oracle)	4.29	0	4.29	0	3.01	0	3.01	0		
GREYFILL	154.6	0.353	98.75	0.250	173.65	0.3770	124.32	0.2631		
LaMa	6.22	0.041	<u>5.61</u>	0.052	n/a	n/a	n/a	n/a		
Palette	6.78	<u>0.049</u>	6.78	<u>0.068</u>	n/a	n/a	n/a	n/a		
Repaint	13.25	0.060	12.21	0.080	8.23	0.047	8.14	<u>0.062</u>		
MCG	7.71	0.062	5.97	0.073	8.43	0.059	6.52	0.065		
combine-noisy	13.48	0.090	9.35	0.099	11.1	0.070	9.78	0.081		
combine-image	11.19	0.096	7.49	0.102	<u>7.89</u>	0.080	<u>5.96</u>	0.089		
GradPaint (ours)	6.613	0.060	5.39	0.069	5.13	0.051	4.29	0.077		

Table 9. Evaluation of various methods on FFHQ and CelebaHQ datasets for *thin* and *medium* masks. Rows COPY (oracle) and GREYFILL are respectfully the lower and upper bounds for LPIPS and FID. LaMa and Palette are both training-based methods. RePaint, *combine-noisy*, *combine-image*, MCG and GradPaint are all training-free methods which all use the same model based on guided diffusion. Best score is shown in **bold** and second best underlined.

to the baselines *combine-image*, *combine-noisy*, LaMa, and RePaint. Baselines *combine-noisy* and *combine-image* clearly have harmonization issues. LaMa tends to have blurry artifacts typical of GANs in the generated areas. RePaint generally produces realistic generations, but which aren't always coherent with other elements of the image. Our method produces high-quality results at a much smaller computational cost than RePaint.

Fig. 13 shows additional select examples on FFHQ dataset. Notice that LaMa produces results close to the reference image, but generally containing blurry artifacts, explaining the generally higher LPIPS scores but lower FID scores than our method. RePaint's method, despite requiring over 5 minutes of compute time for a generation, produces smooth local



Figure 11. Qualitative results with thin masks. Best viewed zoomed and in color. In (a), notice the quality of the text of the hat, which our method most successfully reconstructs. Notice the background face on the right in (b), which only our method managed to decently generate. Finally, in (c), (d), and (e), methods *combine-noisy* and *combine-image* have harmonization issues (see eyes, cheek/eyebrow, and lips respectively), while our method is on par with the costly RePaint.

changes but often fails to harmonize with the global structure of the image (rows 1, 2, 4, 5). Our method produces high-quality and harmonized results, especially visible when the generation requires surrounding context, such as rows 1 and 5 which necessitate generating glasses.

E. Additional Qualitative experiments with Latent Diffusion Models

Fig. 14 shows visual examples of our inpainting results using latent diffusion models. While the baseline method produces low-quality results, our method produces realistic and harmonized results.

F. Uncurated Results and Limits

We primarily previously showed select results on challenging tasks with masks in key places to better appreciate the differences between methods. Figs. 15, 16, 17, and 18 show uncurated examples from on ImageNet comparing *combine-image*, RePaint, and GradPaint. GradPaint works particularly well when the task requires fine-grained texture alignment (see rows 1, 5, 12, 31) and tends to work significantly better for global image coherence compared to other methods (see rows 2,



Figure 12. Qualitative results with medium masks. Best viewed zoomed and in color. Methods *combine-noisy* and *combine-image* have harmonization issues, particularly in (a) and (b). Notice the badge on the hat in (c) where most methods fail to realistically integrate it with the hat. In (d), our method most successfully generates an eye which matches with the input eye. Finally, all methods struggle with the difficult example (e), as it is poorly represented in the training distribution. Nevertheless, our method is the sole one which attempts to reconstruct the hand as a separate entity from the face.

4, 6, 29, 36, 37). However, GradPaint sometimes fails with difficult tasks with unstandard context (see rows 14, 36). From time to time, we see that GradPaint may slightly add unneeded bias to the inpainting task from the background, e.g. row 41 produced a dog with a pink nose, influenced by the pink background. In general, GradPaint works better than RePaint, even though RePaint requires 5x the compute time (or 7x the compute time with the modified GradPaint presented in B).

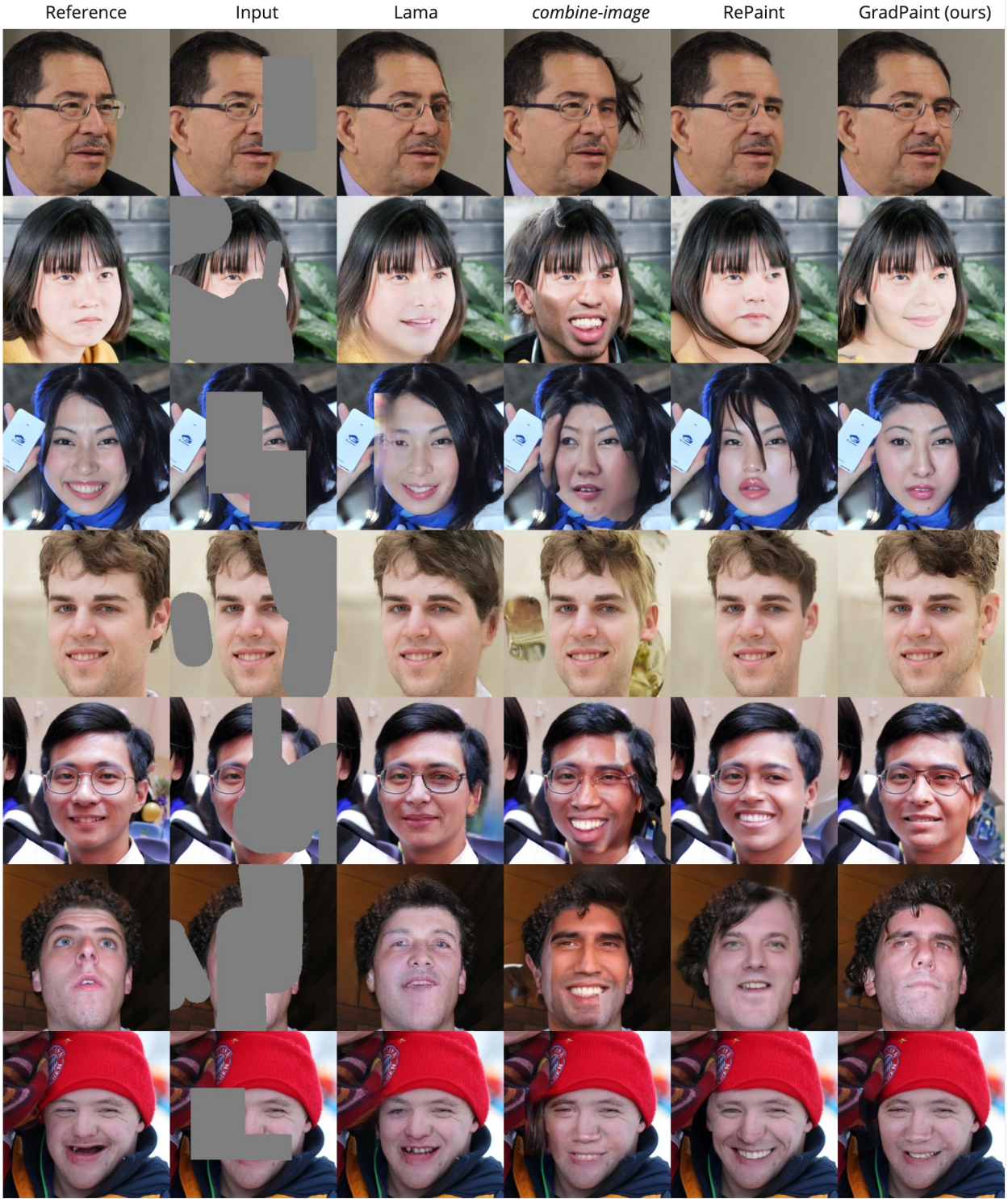


Figure 13. Inpainting results on select images from FFHQ. Best viewed zoomed and in color. Notice that while the overall reconstruction of LaMa is decent, zooming on the image unveils visible blurry and unrealistic artifacts typical of GANs. Results using the *combine-image* baseline are of poor quality with an obvious “copy/paste” effect at the mask. Notice that even with the 4500 forward passes necessary for RePaint, the overall image coherence often fails, despite the high-quality local generation. Our method produces high-quality generation while matching with the global structure of the rest of the image. All models were trained on CelebAHQ dataset.

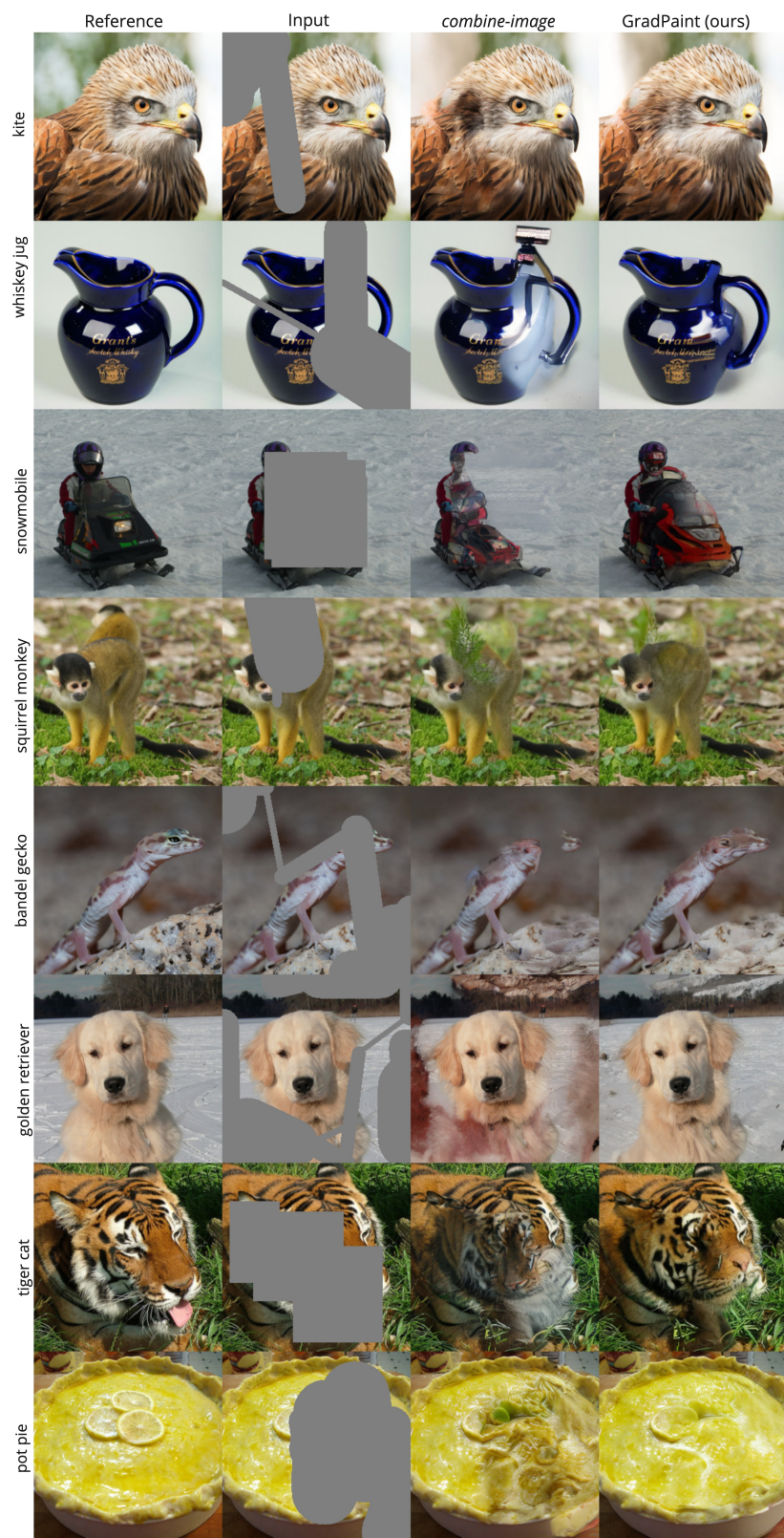


Figure 14. Qualitative examples from ImageNet with the latent diffusion model. Both the baseline and our algorithm are initialized with the same initial noise map.

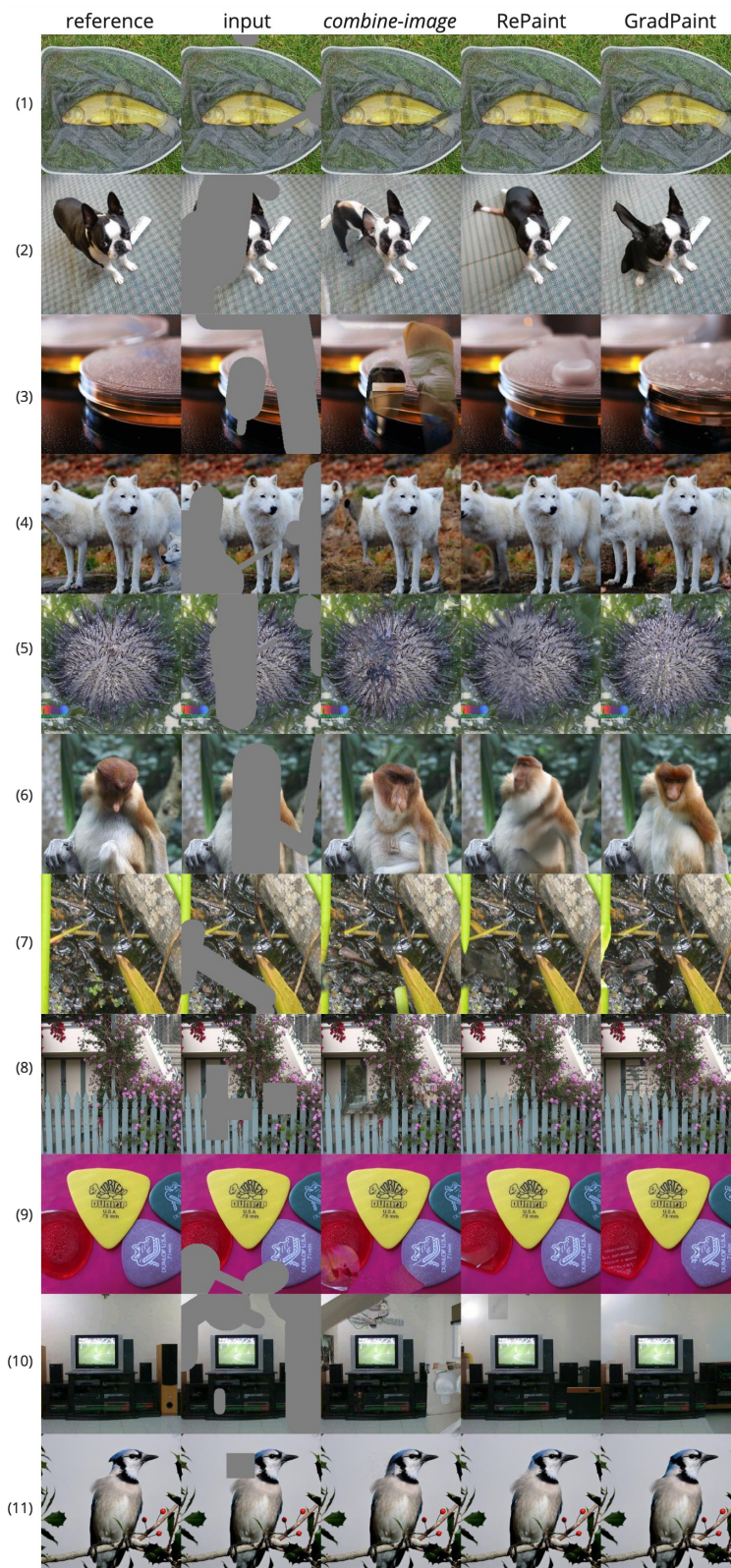


Figure 15. Uncurated results on ImageNet (1). Rows 1, 2, 4, 5, 6 display the superior ability of GradPaint to align fine details and global coherence.

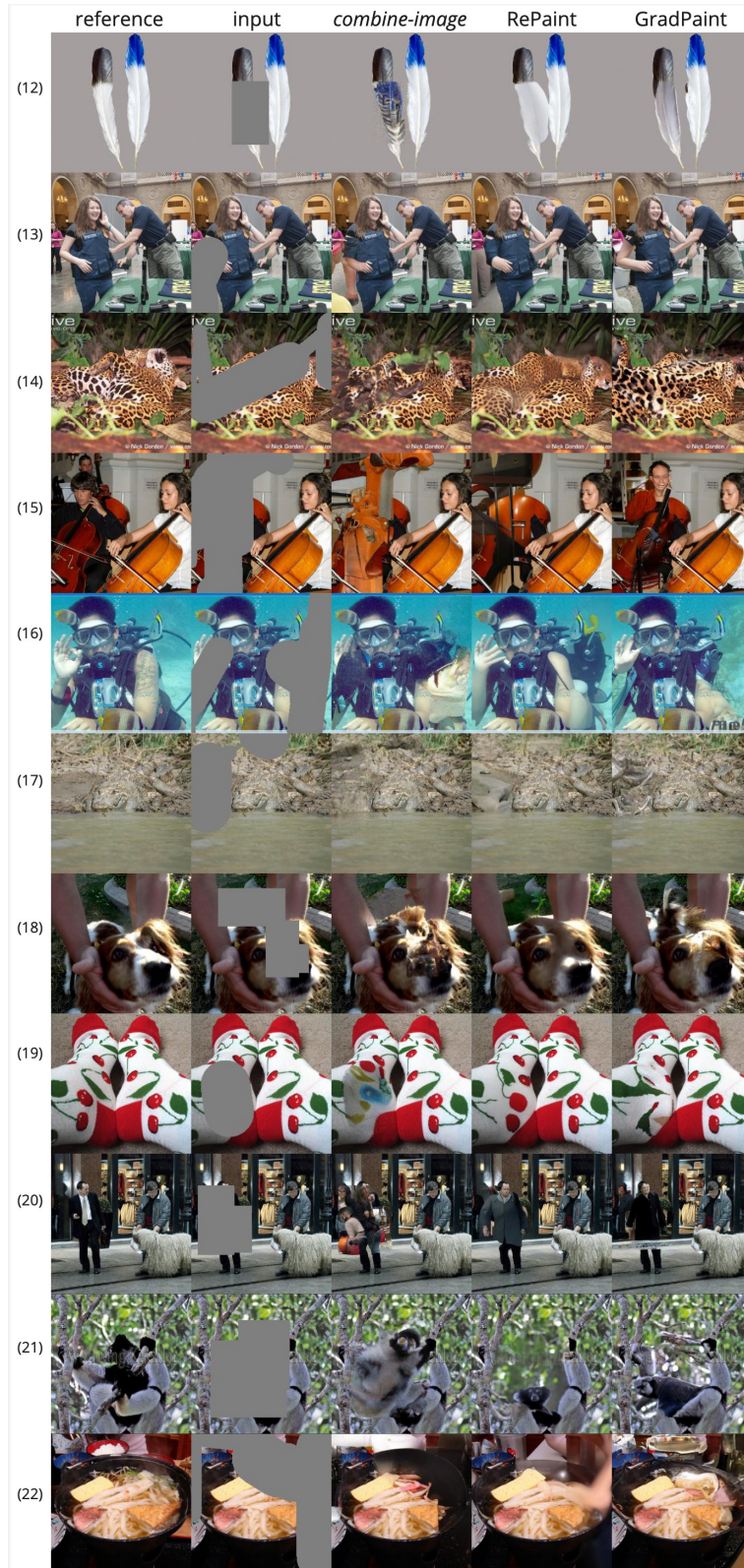


Figure 16. Uncurated results on ImageNet (2). GradPaint works well on alignment tasks (row 12), but sometimes struggles with non-standard input (row 14).

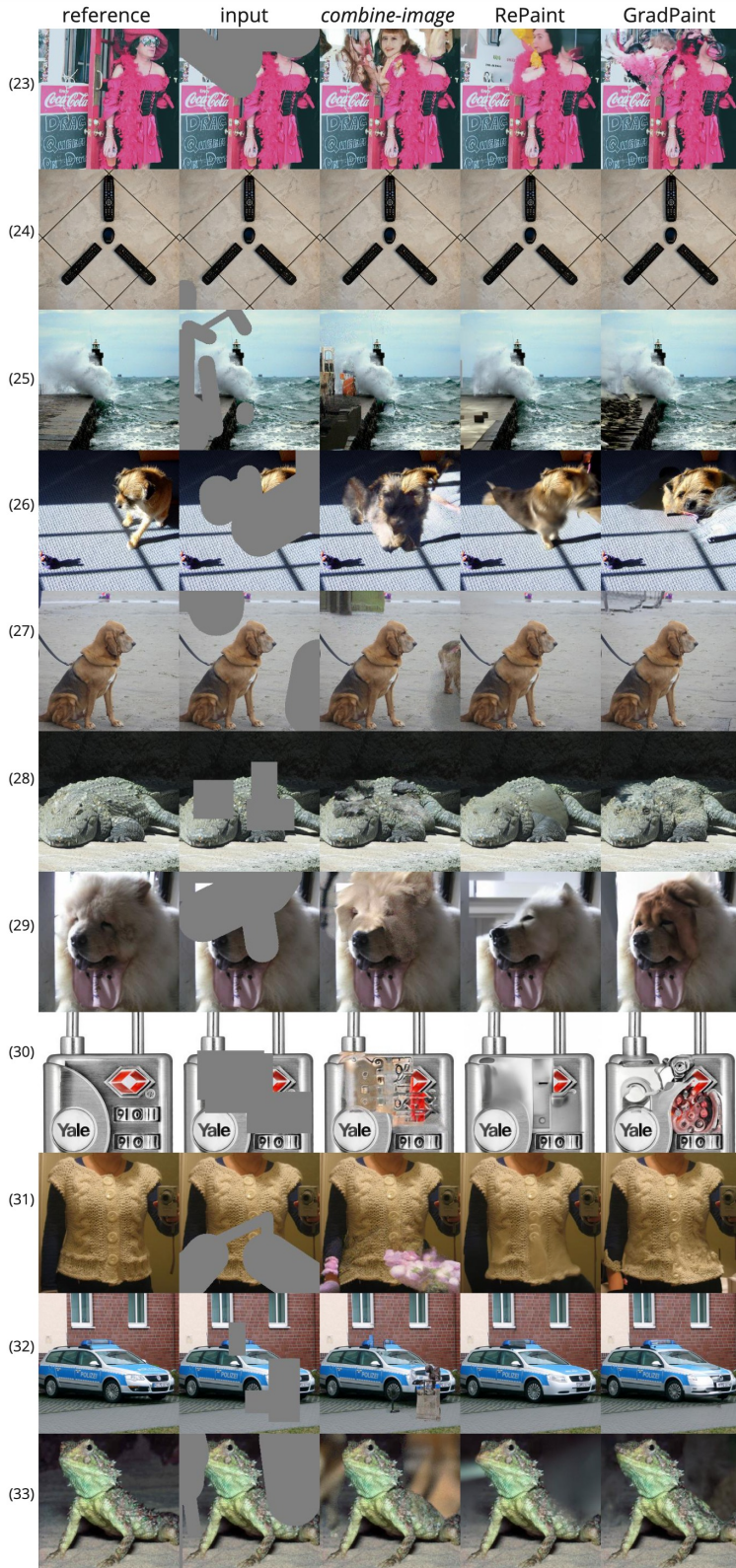


Figure 17. Uncurated results on ImageNet (3). Our method works well on global coherence (row 29) and generating fine textures requiring alignment (row 31).

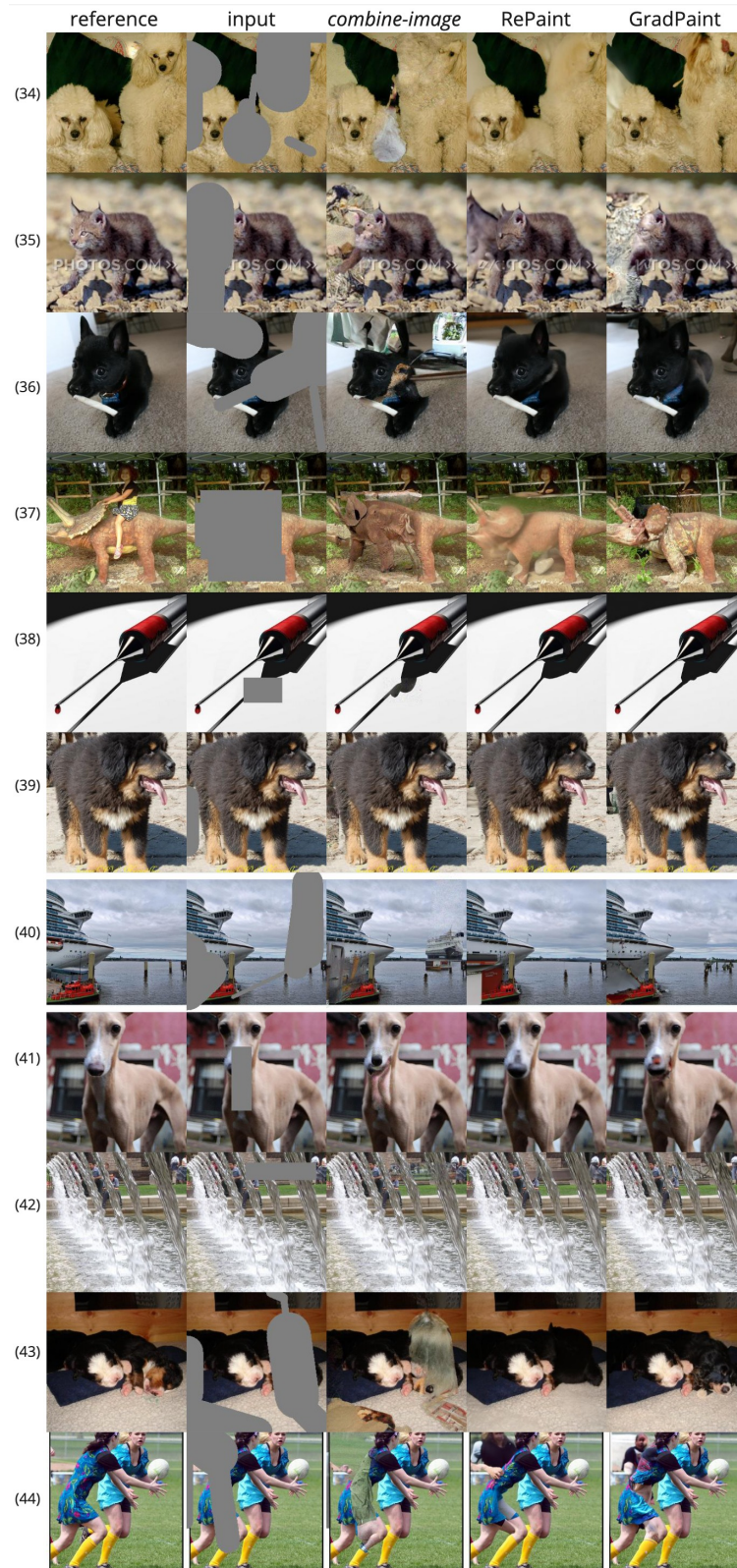


Figure 18. Uncurated results on ImageNet (4). Our method works well on global coherence (rows 36, 37) but sometimes fails on challenging tasks (row 35). From time to time, the background of the image may poorly influence the content to be generated (row 41).